Rotary Balance Wind Tunnel Testing for the FASER Flight Research Aircraft

Casey Denham*
Virginia Tech, Blacksburg, VA, 24061

and

D. Bruce Owens+
NASA Langley Research Center, Hampton, VA, 23681

Abstract

Flight dynamics research was conducted to collect and analyze rotary balance wind tunnel test data in order to improve the aerodynamic simulation and modeling of a low-cost small unmanned aircraft called FASER (Free-flying Aircraft for Sub-scale Experimental Research). The impetus for using FASER was to provide risk and cost reduction for flight testing of more expensive aircraft and assist in the improvement of wind tunnel and flight test techniques, and control laws. The FASER research aircraft has the benefit of allowing wind tunnel and flight tests to be conducted on the same model, improving correlation between wind tunnel, flight, and simulation data. Prior wind tunnel tests include a static force and moment test, including power effects, and a roll and yaw damping forced oscillation test. Rotary balance testing allows for the calculation of aircraft rotary derivatives and the prediction of steady-state spins. The rotary balance wind tunnel test was conducted in the NASA Langley Research Center (LaRC) 20-Foot Vertical Spin Tunnel (VST). Rotary balance testing includes runs for a set of given angular rotation rates at a range of angles of attack and sideslip angles in order to fully characterize the aircraft rotary dynamics. Tests were performed at angles of attack from 0 to 50 degrees, sideslip angles of -5 to 10 degrees, and non-dimensional spin rates from -0.5 to 0.5. The effects of pro-spin elevator and rudder deflection and pro- and anti-spin elevator, rudder, and aileron deflection were examined. The data are presented to illustrate the functional dependence of the forces and moments on angle of attack, sideslip angle, and angular rate for the rotary contributions to the forces and moments. Further investigation is necessary to fully characterize the control effectors. The data were also used with a steady state spin prediction tool that did not predict an equilibrium spin mode.

Nomenclature

b	=	wing span
c.g.	=	center of gravity
C_L	=	lift coefficient
C_l	=	rolling moment coefficient
C_m	=	pitching moment coefficient
C_n	=	yawing moment coefficient
$C_R \equiv \frac{F_R}{1/2 \rho v^2 S}$	=	radial force coefficient
$C_T \equiv \frac{F_T}{1/2 \rho v^2 S}$	=	tangential force coefficient

* Graduate Student, Virginia Tech, Student Member
+ Senior Engineer, Flight Dynamics Branch, M/S 308, Associate Fellow

$C_V \equiv \frac{F_V}{1/2 \rho v^2 S}$	=	vertical force coefficient
F_R, F_T, F_V	=	force components in X, Y, Z directions, respectively
$\hat{\imath}, \hat{\jmath}, \hat{k}$	=	unit vectors in x, y, z directions, respectively
$\hat{I}, \hat{J}, \hat{K}$	=	unit vectors in X,Y, Z directions, respectively
I_x, I_y, I_z	=	aircraft mass moments of inertia in x, y, z directions, respectively
p	=	body axis roll rate
q	=	body axis pitch rate
Q	=	tunnel dynamic pressure
r	=	body axis yaw rate
R	=	spin radius. Distance from c.g. to spin axis
$\frac{2R}{b}$	=	non-dimensional spin radius
$Re \equiv \frac{V\bar{c}}{\nu}$	=	Reynolds number based on mean aerodynamic chord
S	=	wing area
$\bar{V}$	=	freestream velocity vector
V_R, V_T, V_V	=	velocity components in X, Y, Z directions, respectively
$V_v\sqrt{\frac{2}{bg}}$	=	non-dimensional descent velocity
α	=	angle of attack
β	=	angle of sideslip
$\Delta C_l \equiv C_l\|_\Omega - C_l\|_{\Omega=0}$	=	rolling moment contribution due to angular rate
$\Delta C_m \equiv C_m\|_\Omega - C_m\|_{\Omega=0}$	=	pitching moment contribution due to angular rate
$\Delta C_n \equiv C_n\|_\Omega - C_n\|_{\Omega=0}$	=	yawing moment contribution due to angular rate
$\mu \equiv \frac{m}{\rho S b}$	=	relative density of aircraft, non-dimensional mass
ν	=	kinematic viscosity
σ	=	helix angle
ψ, φ, α'	=	aircraft attitude angles in earth frame
$\bar{\Omega}$	=	angular velocity about spin axis
$\frac{\Omega b}{2V}$	=	non-dimensional angular rate, 'spin parameter'
spin axis	=	center of aircraft rotation during a spin

I. Introduction

The Free-flying Aircraft for Sub-scale Experimental Research, or FASER, project is designed to reduce the gap between the demand for increased accuracy in aircraft modeling and simulation and the desire to reduce the cost and complexity of generating these models. By providing a low-cost and low risk platform that enables direct comparisons between wind tunnel, simulation, and flight test data, FASER allows for the improvement of test techniques, modeling and simulation, and aids in the creation of improved control laws[1]. There have been a number of wind tunnel tests completed on the FASER aircraft, including static and forced oscillation wind tunnel tests[2]. Flight tests exploring the full envelope, including high angle of attack and spin maneuvers were also completed[1].

Rotary balance wind tunnel testing grew out of rudimentary spin testing that began at NACA Langley in the 1920s. While wartime testing focused on military configurations, peacetime offered researchers the opportunity to establish testing and modeling techniques and exploration of dynamic scaling effects[3]. Current rotary tests at LaRC are completed in the 20-Foot Vertical Spin Tunnel (VST), which has the capability to perform a variety of free flight and captive tests, including forced oscillation, rotary balance, free-spin characterization and spin recovery testing[3]. Rotary balance testing was first introduced to the LaRC VST after World War II and allowed for the collection of numerical aerodynamic data in contrast to the photographic data collected previously[3]. This led to a series of design recommendations for general aviation aircraft in order to reduce spins with unfavorable spin and recovery characteristics[3]. Spin and rotary testing became increasingly common and more important during the early days of the fighter program in the 1970s due to the longer fuselages and increased variety in mass properties of the new aircraft, as well as the increase in computing power for data storage an analysis[3,4]. Rotary balance testing allows for the prediction of steady state spin characteristics in a low cost, low risk environment.

The rotary derivatives, C_{l_Ω}, C_{m_Ω}, and C_{n_Ω}, obtained through a rotary balance wind tunnel test, are necessary in order to better model the aerodynamic properties of the aircraft through spin maneuvers[5]. Rotary balance test data can also be used to predict aircraft steady spin states. One such prediction method is discussed in Ref. 6 and 9. This method simplifies the equations of motion and finds possible steady state spins by finding the angle of attack, sideslip angle, and angular rotation rate that balance the inertial and aerodynamic components of the moments acting on the aircraft[6,7]. Although real aircraft spins are rarely steady state and therefore exhibit some degree of oscillatory behavior, this method uses the average value of α and β over the oscillation cycle[7]. Regardless, this method allows for the prediction of possible spin modes for the FASER aircraft that can then be compared to flight test data.

The nomenclature and coordinate systems used throughout the report are presented first. The model and test apparatus are then presented, including details on the model geometry and wind tunnel rotary balance testing rig. The test instrumentation and data reduction methods are discussed in the test techniques section. A brief summary of the static aerodynamics of the aircraft is also provided. The test parameters, including the development of the test matrix, are presented in the subsequent section. The experimental procedures section details the procedures of how the test was conducted, including instrumentation check out, wind off tares, and wind on runs. It also describes some of the changes made during the test and presents a summary of the data collected. The results and a short discussion are then presented, including a presentation of the rotary balance data as well as the steady state spin prediction for FASER. A summary of the rotary balance test and the conclusions drawn from the results are presented in the final section.

II. Experimental Methods

A. Coordinate Systems

Two coordinate systems are used to describe the aircraft attitude for rotary balance testing – the aircraft frame, denoted by unit vectors $\hat{\imath}, \hat{\jmath}, \hat{k}$ and the earth frame, denoted by unit vectors $\hat{I}, \hat{J}, \hat{K}$. The aircraft frame uses the standard axis system orientation, with the origin at the c.g. and the positive x-axis orientated towards the nose, the positive y axis orientated out the right wing, and the positive z axis orientated downwards, shown in **Error! Reference source not found.**. The earth frame axis system, also shown in **Error! Reference source not found.**, is also defined with the origin at the aircraft c.g. The X axis points horizontally through the centerline of the spin, the Y axis is parallel to the ground (assuming a flat earth) and is tangential to the path of the spin, and the Z axis points towards the ground. Also used are the aircraft angles, ψ, φ, α', which describe the attitude of the aircraft throughout a spin in the aircraft frame. From the initial orientation, ψ is defined along a yaw rotation, with the aircraft then rolling about its current x-axis for the angle φ. α' is then defined as a rotation about the aircraft's current y axis. Positive rotation angles follow the right-hand-rule.

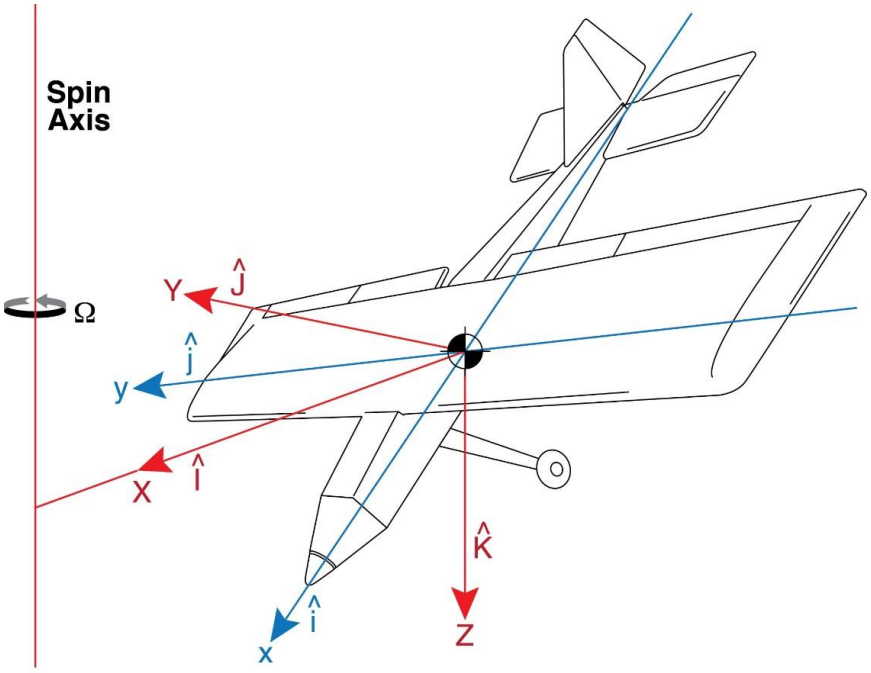

Figure 1. Aircraft and Earth axis frames for FASER.

B. Model

A rotary balance wind tunnel test was conducted of the 6.3 ft. wingspan FASER model, shown in **Error! Reference source not found.**, before a previous flight test, and in **Error! Reference source not found.** in the 20-Foot Vertical Spin Tunnel. For wind tunnel testing, the motor and air data probes were removed. The aircraft is a commercially available radio controlled Hangar 9 ARF Ultra-Stick™ 120 kit-built tail-dragger. The size allows for flight testing and wind tunnel testing to be conducted on the same model. Key aircraft parameters are presented in **Error! Reference source not found.**.

This model has previously undergone numerous wind tunnel tests in the NASA LaRC 12-Foot Low Speed Tunnel (LST) as well as numerous flight tests. Modifications to the original aircraft frame were made for these wind tunnel tests. For the rotary balance test additional bulkheads, mounting plates, and a mounting block, as shown in **Error! Reference source not found.**, were added in order to allow for installation of a six-component strain gauge balance.

Figure 3. FASER Aircraft shown before a previous flight test.

Figure 2. FASER Aircraft in the VST in the 0° angle of attack configuration.

Table 1. FASER Aircraft Properties

Geometric Characteristics[1,2]	
Wing Span, ft.	6.29
Reference Wing Area, ft^2	8.28
Aspect Ratio	4.42
Mean Aerodynamic Chord, ft.	1.42
As Flown Mass Properties[1]	
Weight, lbf.	19.72
$\frac{x_{cg}}{\bar{c}}$	0.25
$\frac{y_{cg}}{b}$	0
$\frac{z_{cg}}{\bar{c}}$ above the bottom of the fuselage at $\frac{x_{cg}}{\bar{c}}$	0.165
I_x, slug-ft^2	0.496
I_y, slug-ft^2	0.656
I_z, slug-ft^2	1.164
I_{xz}, slug-ft^2	0.560

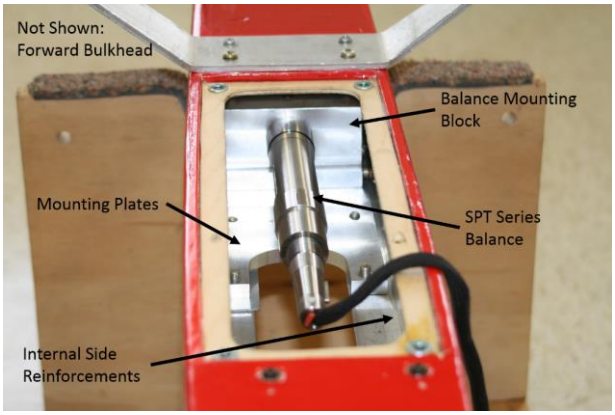

Figure 4. Internal structure of FASER wind tunnel model, as seen from bottom of aircraft.

C. Facility Description

The aircraft was tested in the NASA LaRC 20-Foot Vertical Spin Tunnel (VST). The VST is an atmospheric, low-speed, annular return tunnel with a 20 foot diameter and 25 foot tall test section, as shown in **Error! Reference source not found.**. For rotary balance testing in the VST, the model is mounted on a sting attached to a rotation arm capable of rotating the model with positive or negative spin rates[7].

III. Test Technique

Rotary balance wind tunnel testing consists of rotating the model at various angular rotation rates for a range of angles of attack and sideslip angles. Aircraft forces and moments are measured using an internally mounted six component strain gauge balance. A typical run consists of varying the angular rate for each angle of attack, while keeping sideslip angle constant. Both positive (clockwise) and negative (counterclockwise) angular rates are used in order to allow for comparison and verification.

As rotating the model in a vacuum in order to determine the weight and inertial effects is impractical, tares are taken with the model enclosed in a large "tare bag", as shown in **Error! Reference source not found.**, with the wind off. A tare must be taken for each angle of attack, sideslip angle, and angular rate combination[5]. The tare bag allows the air surrounding the model to rotate at the same angular rate as the model, reducing wind-off aerodynamic effects[7].

For the rotary test, the aircraft is moved into the desired angle of attack and sideslip angle and then rolled and translated radially in the tunnel so that the spin axis remains constant through the c.g. for all attitudes. It is then rotated at the desired angular rates, starting at 0 and increasing through positive rates, then decreasing through negative rates. The sideslip angles used in the test ranged from -5 to 10 degrees and angles of attack ranged from 0 to 50 degrees. Reduced angular rates ranged from -0.5 to 0.5 for angles of attack greater than or equal to 10 degrees. Control surface deflections were tested for sideslip angles of -5, 0 and 10 degrees.

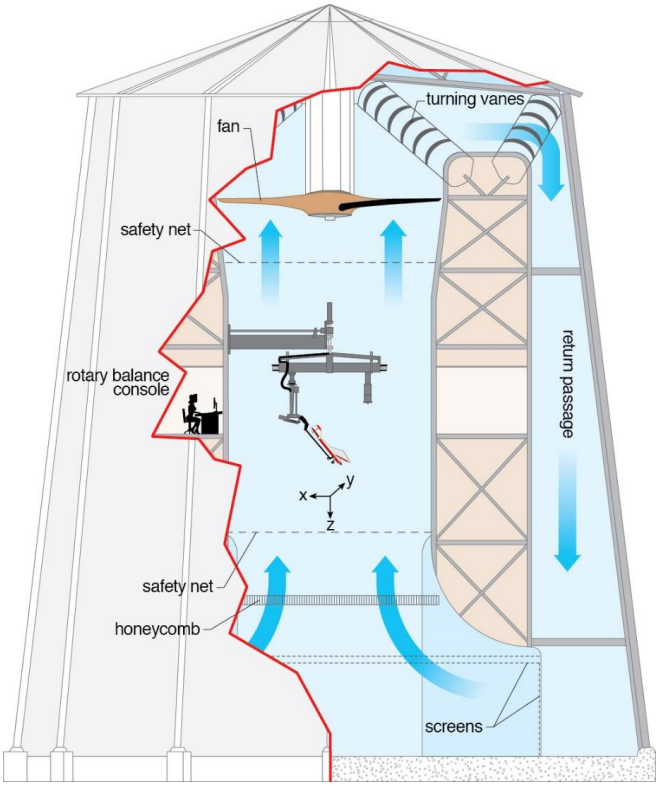

Figure 5. Cross-section of the 20-Foot Vertical Spin Tunnel, showing the rotary balance apparatus and placement of the model in the tunnel.

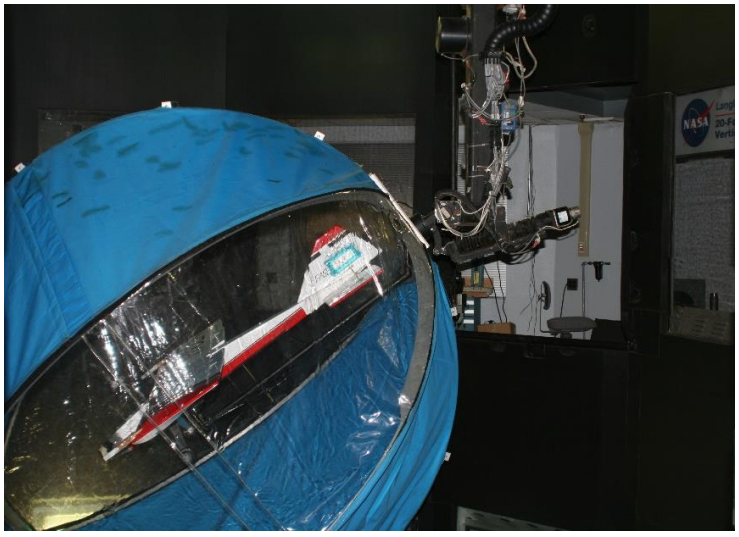

Figure 6. FASER inside the rotary tare bag.

A. Data Comparison

The static data from the rotary test in the VST were compared to previous tests conducted in the 12-Foot LST to ensure that there were no significant differences before proceeding with the rotary balance test. The rotary balance test was conducted at Q = 1 psf (Re ≈ 240k based on wing mean aerodynamic chord), due to balance load limit constraints and to match flight angular rate similitude requirements, while prior tests were completed in the 12-Foot LST from Q = 2 psf (Re ≈ 340k) to Q = 4 psf (Re ≈ 470k). These static tests demonstrated that Reynolds number effects were minimal between Q = 2 psf (V = 40 ft/s) and the flight velocity of 60 ft/s (Q ≈ 4 psf), as shown in **Error! Reference source not found.**. Static runs in the VST were completed at Q = 2 psf and Q = 1 psf in order to determine the effects of Reynolds number within this range. **Error! Reference source not found.** shows a good agreement between the test conducted in the VST (Q = 1 psf) and previous tests conducted in the 12-Foot LST (Q = 2 psf). **Error! Reference source not found.** and **Error! Reference source not found.** show that other forces and moments also agreed well across the different tests, wind tunnels, and dynamic pressures. In **Error! Reference source not found.**, the 12-Foot LST yawing moment data differs in sign from the VST data in the 14° to 20° degree range. This behavior is not uncommon on aircraft where one wing will stall before the other. The difference in sign of the yawing moment even exists in repeat runs conducted in the 12-Foot LST test. Because of the agreement between Q = 1 psf and Q = 2 psf, and Q = 2 psf and Q = 4 psf, the wind tunnel data for Q = 1 psf should be a good approximation of the data taken at the flight velocity.

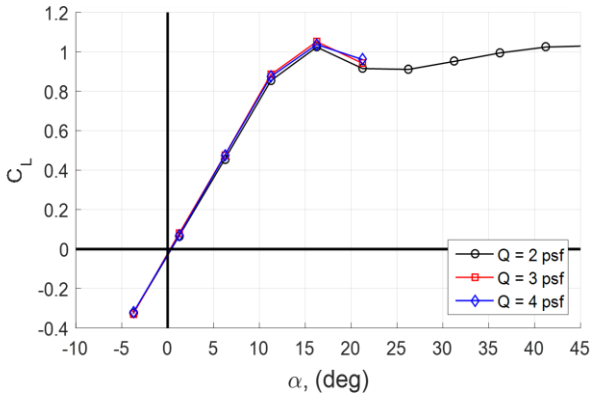

Figure 7. Comparison of dynamic pressure effects in the 12-Foot LST.

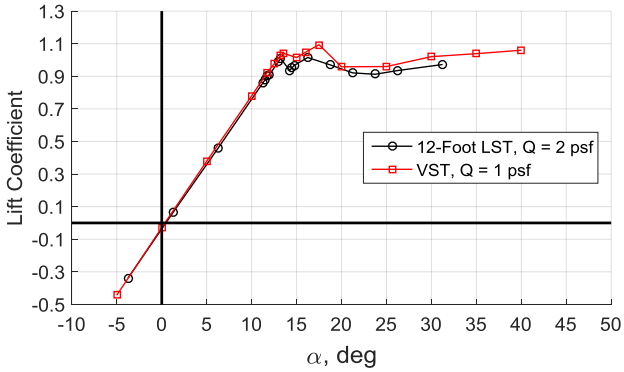

Figure 8. Comparison of lift coefficient between the rotary balance test and additional previous static data[2].

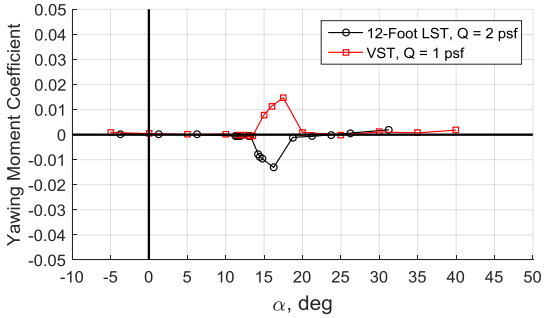

Figure 9. Comparison of yawing moment coefficient between the rotary balance test and previous static data[2].

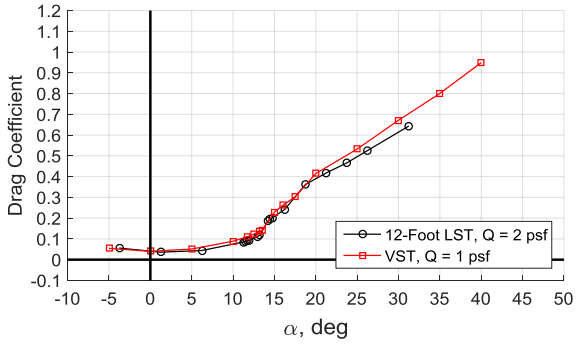

Figure 10. Comparison of drag coefficient between the rotary balance test and previous static data[2].

B. Steady State Spin Prediction

The steady state spin prediction method discussed below is summarized from Ref. 6. The algebraic description is provided here with the process shown graphically in **Error! Reference source not found.** to **Error! Reference source not found.**. The prediction method is based on simultaneously satisfying equilibrium between aerodynamic moments and inertial moments for all three moment equations: roll, pitch, and yaw.

Step 1: (**Error! Reference source not found.**): for each α' and φ tested, any value of the non-dimensional angular rate $\frac{\Omega b}{2V}$ that satisfies both the calculated inertial pitching moment, $C_{m_{inertial}}$ (Eq. 1), and the measured aerodynamic pitching moment, $C_{m_{aero}}$, corresponds to a possible steady spin mode.

Step 2: (**Error! Reference source not found.**): for each α', φ and $\frac{\Omega b}{2V}$ triplet, find the value of rolling moment C_l that satisfies $C_{l_{inertial}}$(Eq. 2) and $C_{l_{aero}}$. For all α' tested, plots of φ vs α' and $\frac{\Omega b}{2V}$ vs α'are made to quickly identify potential spin states, or states when two of the three moment equilibriums are satisfied, as shown in **Error! Reference source not found.** and **Error! Reference source not found.**.

Step 3: (**Error! Reference source not found.**): the value of α' that satisfies $C_{n_{aero}}$ and $C_{n_{inertial}}$, calculated with Eq. 4, using the corresponding values of $\frac{\Omega b}{2V}$ and φ for each α', signifies a prospective spin state that satisfies equilibrium for all three moment equations. Each prospective spin state must then be classified as stable or unstable. The classification is determined by comparing the slope of the $C_{n_{inertial}}$vs $\alpha^{'}$ to the $C_{n_{aero}}$ vs $\alpha^{'}$ slope at the crossing of the two lines. A stable spin state is indicated when $C_{n_{inertial}}$vs $\alpha^{'}$ slope is positive and the $C_{n_{aero}}$ vs $\alpha^{'}$ slope is negative at the intersection point. If this condition is not met, then the equilibrium is unstable and the method is unable to identify a steady-state spin. A stable spin state is shown in **Error! Reference source not found.**. Once α', φ, and $\frac{\Omega b}{2V}$ for the steady spin state are known, aircraft coefficients can be transformed into the earth reference frame, using Eq. 5, and the spin radius, the helix angle, σ, and ψ can then be calculated using Eq. 6 to 8. In order to calculate the spin radius the aircraft relative density, μ, is determined using Eq. 9.

It is important to note that for the LaRC VST, a model is assumed to be descending vertically, so that $\frac{\Omega b}{2V}$ is made non-dimensional using V_v, the tunnel vertical component of velocity, instead of the total aircraft velocity, V, and is accounted for in all equations. In theory, only one direction of rotation (either positive or negative angular rates) is analyzed since a spin with negative sideslip and positive spin rate should have a mirror spin with positive sideslip and negative spin rate for neutral controls and pro-spin controls induce a spin in a single direction. However, in practice, large deviations can be seen between these spins, so both subsets of data should be analyzed for potential spin states. This method is intended to find steady state spins and therefore is unable to fully characterize unsteady or oscillatory spins.

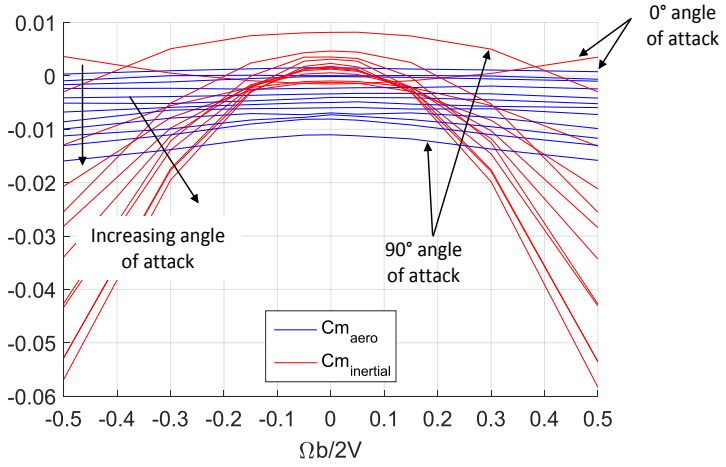

Figure 11. Example of aerodynamic (blue) and inertial (red) pitching moment coefficient equilibrium for a range of angles of attack.

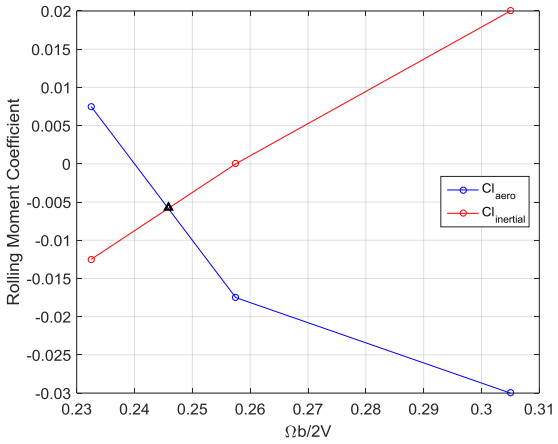

Figure 14. Example of aerodynamic (blue) and inertial (red) rolling moment coefficient equilibrium.

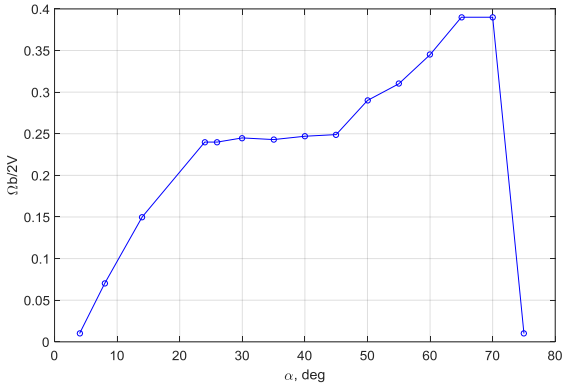

Figure 13. Example $\frac{\Omega b}{2V}$ vs α, from rolling moment coefficient equilibrium.

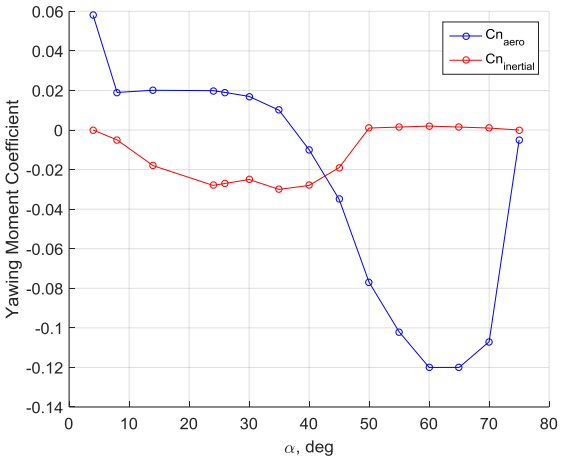

Figure 12. Example of aerodynamic (blue) and inertial (red) yawing moment coefficient equilibrium and of a steady state spin, indicated by the positive slope of inertial yawing moment and the negative slope of the aerodynamic yawing moment at the equilibrium point.

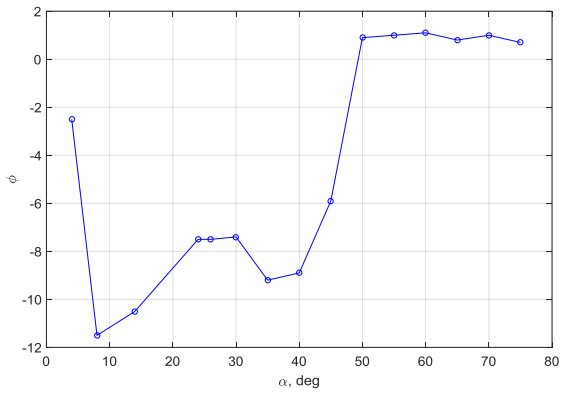

Figure 15. Example of φ vs α, from rolling moment coefficient equilibrium.

$$C_{m_{inertial}} = -\frac{4\mu b}{\bar{c}}\left(\frac{I_z - I_x}{mb^2}\right)\cos^2\varphi \sin 2\alpha' \left(\frac{\Omega b}{2V}\right)^2$$

(Equation 1)

$$C_{l_{inertial}} = 4\mu\left(\frac{I_z - I_y}{mb^2}\right)\sin 2\varphi \sin\alpha' \left(\frac{\Omega b}{2V}\right)^2$$

(Equation 2)

$$\varphi = \frac{1}{2}\sin^{-1}\left\{\frac{C_{l_{inertial}}}{4\mu\left(\frac{I_z - I_y}{mb^2}\right)\sin\alpha'\left(\frac{\Omega b}{2V}\right)^2}\right\}$$

(Equation 3)

$$C_{n_{inertial}} = 4\mu\left(\frac{I_y - I_x}{mb^2}\right)\sin 2\varphi \cos\alpha' \left(\frac{\Omega b}{2V}\right)^2$$

(Equation 4)

$$\bar{F} = (F_x \sin\alpha' - F_z \cos\alpha')\bar{I} + \left(-F_x \sin\varphi \cos\alpha' + F_y \cos\varphi - F_z \sin\varphi \sin\alpha'\right)\bar{J} + \left(F_x \cos\varphi \cos\alpha' + F_y \sin\varphi + F_z \cos\varphi \sin\alpha'\right)\bar{K} = F_R\bar{I} + F_T\bar{J} + F_V\bar{K}$$

(Equation 5)

$$\frac{2R}{b} = \frac{C_R}{4\mu\left(\frac{\Omega b}{2V}\right)^2}$$

(Equation 6)

$$\sigma = \tan^{-1}\left(\frac{\Omega b}{2V}\frac{2R}{b}\right)$$

(Equation 7)

$$\psi = -\tan^{-1}\left(\frac{C_T}{C_R}\right)$$

(Equation 8)

$$\mu = \frac{m}{\rho S b}$$

(Equation 9)

C. Test Parameters

Data from a FASER flight test were used in an attempt to determine the characteristics of the observed spin in order to generate a test matrix and provide a comparison to the steady state spin prediction results[1]. In flight, by simply stalling the airplane with full up elevator then applying full rudder deflection, FASER would enter a steep spin with high roll rate (>200 deg/sec), oscillatory pitch rate, and moderate yaw rate (~160 deg/sec). The aircraft was equipped to measure α, β, free-stream velocity, angular rates, accelerations, control surface deflections, and GPS position[1]. However, during the spin maneuvers, the roll rate gyro of the inertial measurement unit (IMU) saturated causing the majority of the data to be uncorrectable (**Error! Reference source not found.** and **Error! Reference source not found.**). Flight test video was then analyzed in order to estimate the aircraft total rate of rotation, Ω. This value was then used to approximate the aircraft roll rate in order to correct the angle of attack, sideslip angle, and free-stream velocity, in order to estimate the aircraft spin characteristics presented in **Error! Reference source not found.**.

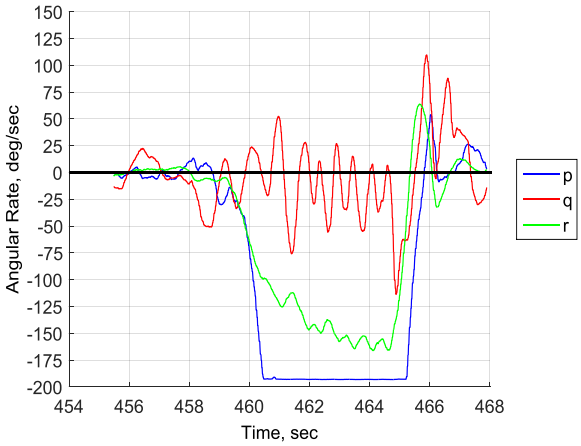

Figure 17. Angular rates during flight test spin maneuver, showing roll rate saturation.

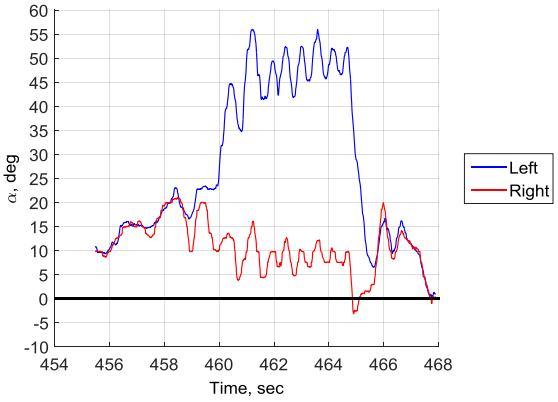

Figure 16. Angle of attack during flight test spin maneuver, showing offset between left and right wingtip air data probes, shown in Error! Reference source not found..

Table 2. FASER flight test spin characteristics estimation.

α	β	Velocity	Ω
30°	5°	100 ft/sec	250 dps

Shown in **Error! Reference source not found.**, the matrix includes an angle of attack range from 0 to 50 degrees, a sideslip range from -25 to 25 degrees, and a reduced angular rate range from -0.5 to 0.5. This angle of attack range was selected based upon the load limits of the balance and the radial translation capabilities of the rotary balance test rig. The sideslip and reduced angular rate ranges were selected based upon historical rotary balance testing techniques and guidelines[8]. A selection of pro- and anti-spin control surface deflections were also tested.

Table 3 - Rotary Balance Test Matrix

alpha \ beta	-25	-20	-15	-12	-8	-4	0	4	8	12	15	20	25
0													
5													
10													
12													
15													
20													
25													
30													
34													
36													
38													
40													
42													
45													
50													

$\frac{\Omega b}{2V}$ = 0, +/-0.05, +/-0.15, +/-0.3, +/-0.5 for every alpha/beta combination

baseline (all controls = 0)
rudder=40, elevator = -25
rudder=40, elevator = -25, aileron Full L+/R-
rudder=40, elevator = -25, aileron Full L-/R+

IV. Results and Discussion

The aircraft forces and moments functional dependence on angle of attack, sideslip angle, angular rate, and control surface deflections will be examined. The rotary balance data will also be used in an attempt to predict steady spin states for FASER. Data for the aircraft moments will be presented first, with the rolling moment coefficient discussed in depth because this moment is the primary driver for airplanes with steep spins, followed by an overview of the pitching moment and yawing moment results. Data for the forces will then be presented, with axial force first, followed by side force and normal force. In order to better observe the rotary contribution to the aircraft aerodynamics the data are presented by subtracting the static values from the measured data. Lastly, the results of the spin prediction method will be discussed.

To establish the effect of angle of attack on rolling moment, various angles of attack were plotted against reduced angular rate as shown in **Error! Reference source not found.**. The angles of attack selected for analysis include 0°, 15° (stall), 25°, 34° (anticipated spin angle of attack), and 50°. For zero degrees angle of attack the data are linear, as expected. At high angles of attack, for small angular rates, there is little functional dependence, while for higher rates there is some degree of functional dependence. The asymmetry in positive and negative rates is most likely due to model asymmetry or flow irregularities. The effect of sideslip is shown in **Error! Reference source not found.**, for the anticipated angle of attack for spin, demonstrating a functional dependence on sideslip angle and angular rate. **Error! Reference source not found.** shows the effect of control surface deflections on rolling moment. A slight dependence on control surface deflections is observed, as well as asymmetry across angular rates.

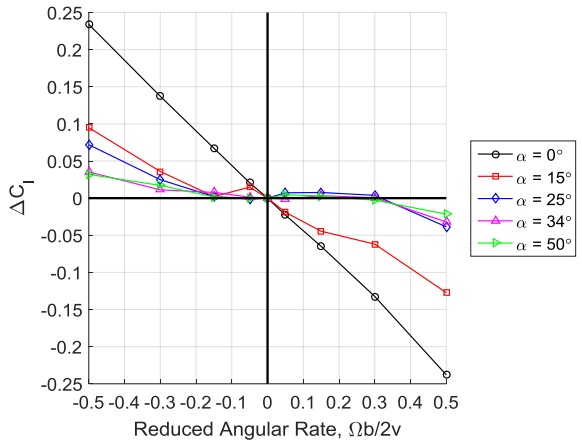

Figure 20. Effect of angle of attack on rolling moment coefficient, showing dependence on angle of attack and angular rate for β=1.3°.

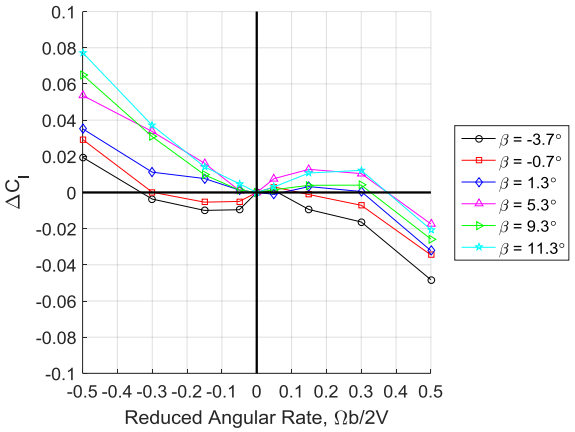

Figure 19. Effect of sideslip on rolling moment coefficient, showing dependence on angular rate and sideslip angle for α=34°.

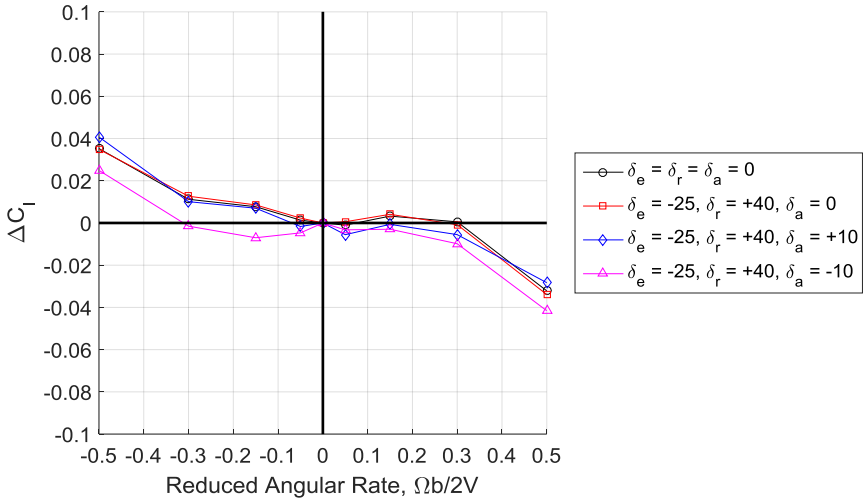

Figure 18. Effect of control deflection on rolling moment coefficient, showing dependence on angular rate and slight dependence on control surface deflection for β=1.3° and α=34°.

The same plots are shown for the pitching moment contribution in **Error! Reference source not found.** to **Error! Reference source not found.**. As with rolling moment, pitching moment has a dependence on both angle of attack, sideslip angle, and angular rate. There is a slight dependence on control surface deflection with the same asymmetries with respect to angular rate as with pitching moment. **Error! Reference source not found.** to **Error! Reference source not found.** show the effects of angle of attack, sideslip angle, and control surface deflections for the yawing moment contribution. The same dependencies on angle of attack, sideslip angle, and angular rate are seen, as well as the asymmetries in the effect of control surface deflection. There are also large asymmetries with respect to angular rate for stall (≈15° angle of attack) and very high angle of attacks. Further investigation is needed to account for the differences seen throughout this range of angle of attack.

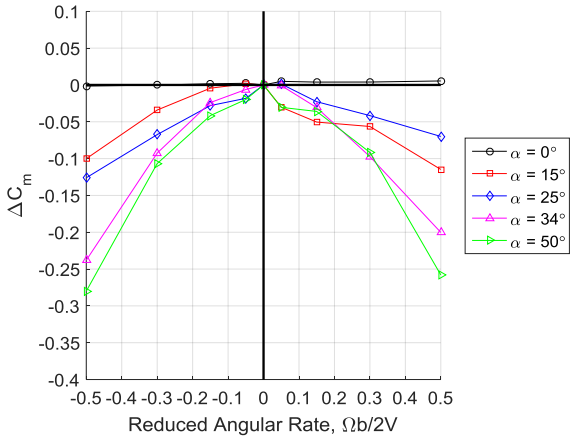

Figure 25. Effect of angle of attack on pitching moment coefficient, showing dependence on angle of attack and angular rate for β=1.3°.

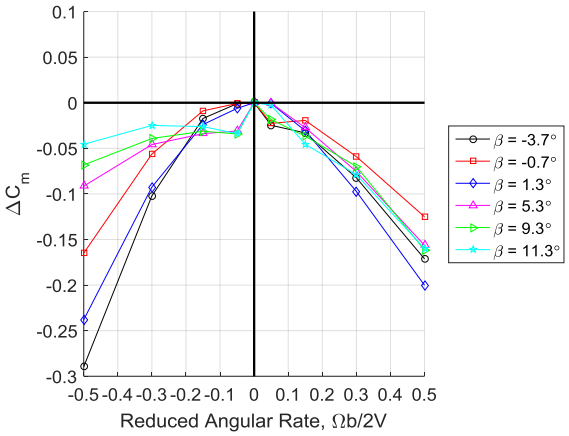

Figure 24. Effect of sideslip on pitching moment coefficient, showing dependence on angular rate and sideslip angle for α=34°.

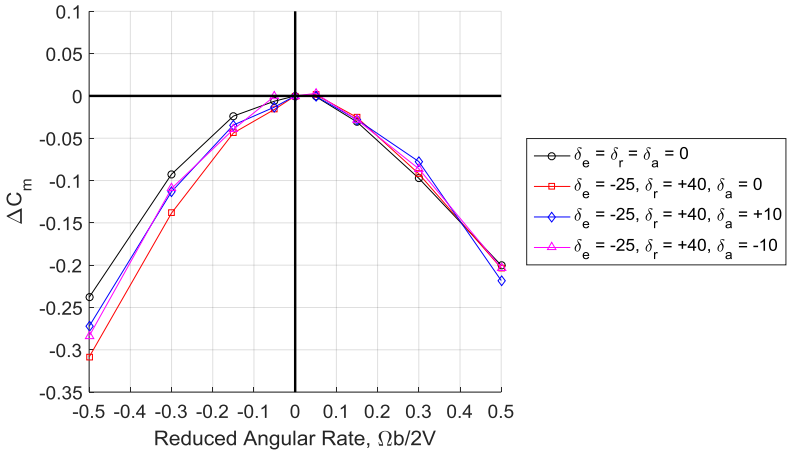

Figure 21. Effect of control deflections on pitching moment coefficient, showing dependence on angular rate and slight dependence on control surface deflection for β=1.3° and α=34°.

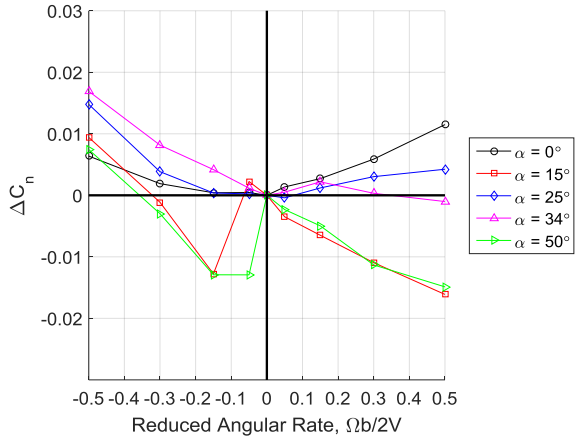

Figure 23. Effect of angle of attack on yawing moment coefficient, showing dependence on angle of attack and angular rate for β=1.3°.

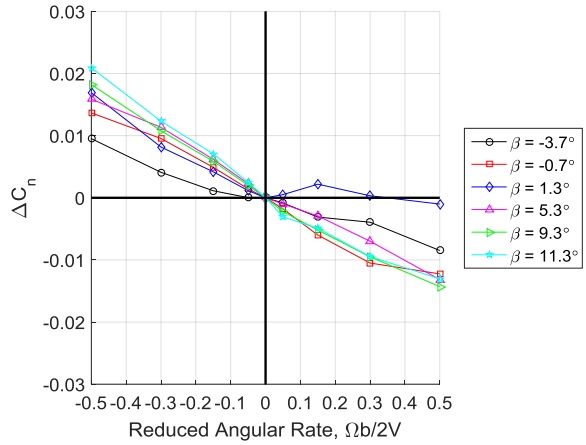

Figure 22. Effect of sideslip on yawing moment coefficient, showing dependence on sideslip angle and angular rate for α=34°.

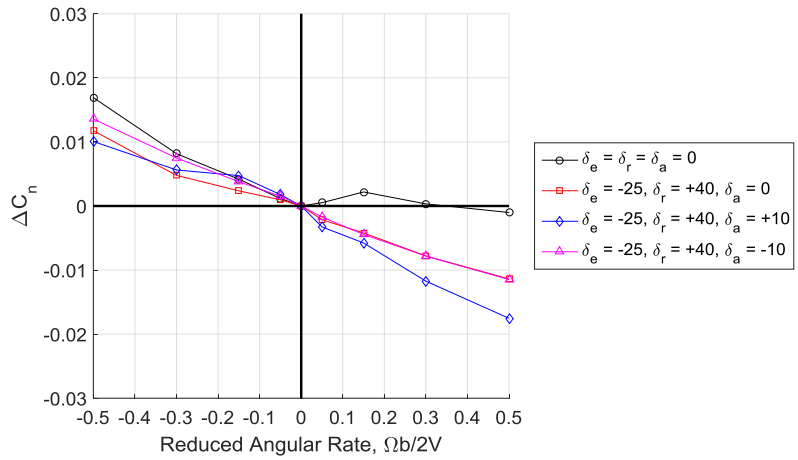

Figure 26. Effect of control deflection on yawing moment coefficient, showing dependence on angular rate and control surface deflection for β=1.3° and α=34°.

The plots for axial force can be seen in **Error! Reference source not found.** to **Error! Reference source not found.**. As with the aircraft moments, there is a functional dependence on angle of attack, sideslip angle, angular rate, and control surface deflection. Angle of attack has minor effects, except for near stall, where it has a large effect. Differences due to positive and negative sideslip angle are likely due to model asymmetries or flow irregularities. At low angular rates, there is little functional dependence on control surface deflections and the dependence is approximately symmetric for positive and negative angular rates.

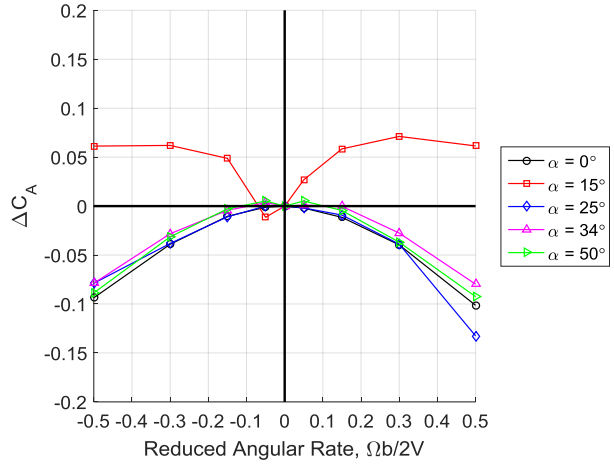

Figure 27. Effect of angle of attack on axial force coefficient, showing large variations near stall for β=1.3°.

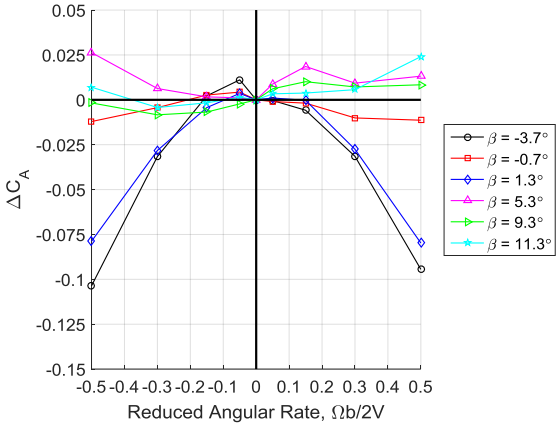

Figure 28. Effect of sideslip angle on axial force coefficient, showing dependence on sideslip angle and angular rate for α=34°.

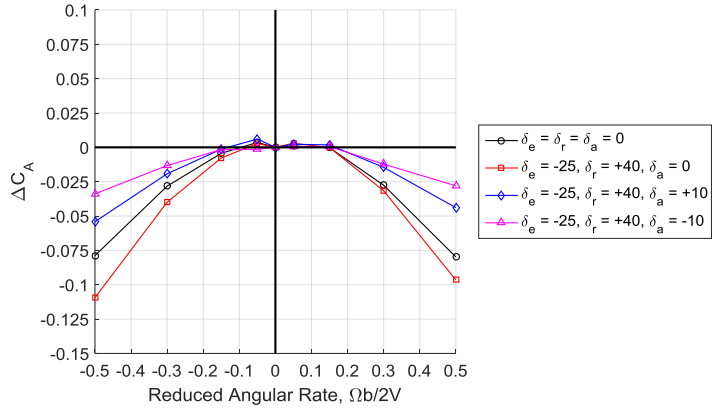

Figure 29. Effect of control surface deflection on axial force coefficient, showing dependence on control surface deflection for β=1.3° and α=34°.

Error! Reference source not found. to **Error! Reference source not found.** show the effect of angle of attack, sideslip angle, angular rate, and control surface deflection on side force coefficient. There is a strong dependence on angle of attack and angular rate, while sideslip angle has asymmetric effects with respect to angular rate. There is a significant effect of aileron deflection, while rudder and elevator have only minor effects. The functional dependencies for normal force coefficient are shown in **Error! Reference source not found.** to **Error! Reference source not found.**. The functional dependence on angle of attack is less pronounced at higher angles of attack and is most pronounced near stall. There is a

large dependence on sideslip angle and angular rate, while control surface deflections have asymmetric effects with respect to angular rate.

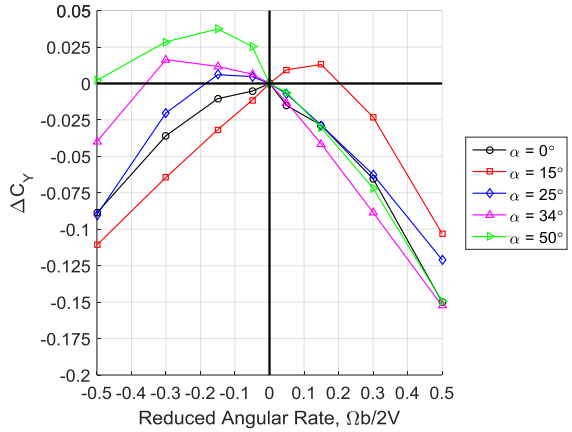

Figure 33. Effect of angle of attack on side force coefficient, showing dependence on angle of attack and angular rate for β=1.3°.

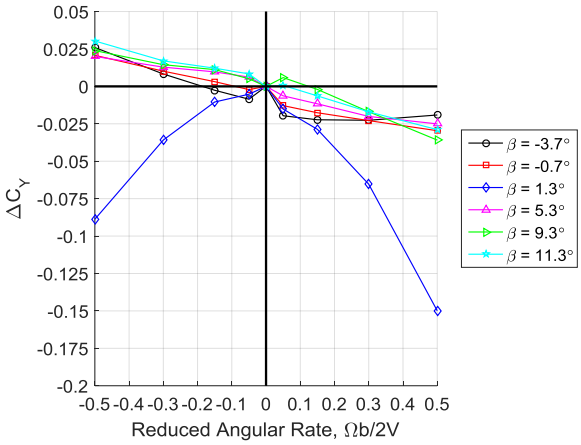

Figure 32. Effect of sideslip angle on side force coefficient, showing asymmetric dependence on sideslip angle and angular rate for α=34°.

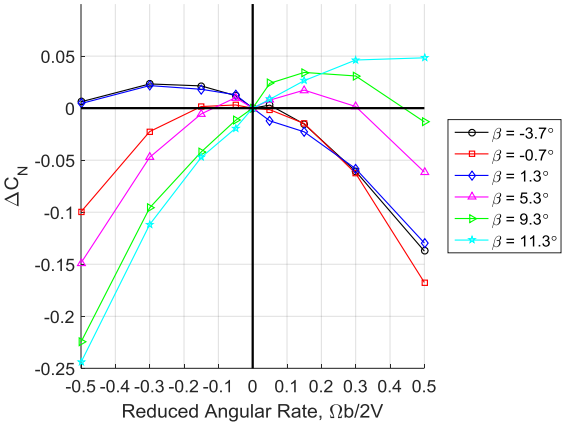

Figure 35. Effect of sideslip angle on normal force coefficient, showing large dependence on sideslip angle and angular rate for α=34°.

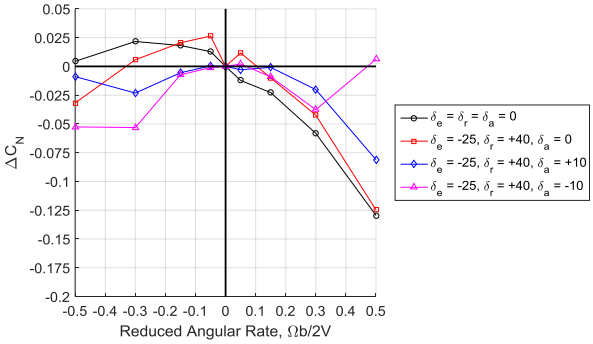

Figure 34. Effect of control surface deflection on normal force coefficient, showing asymmetric dependence on control surface deflection and angular rate for β=1.3° and α=34°.

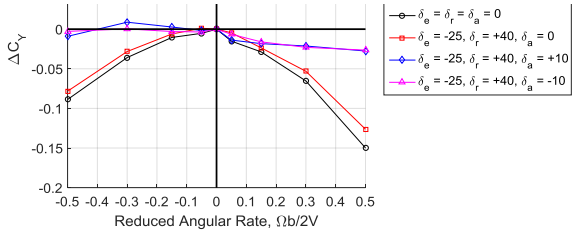

Figure 31. Effect of control surface deflection on side force coefficient, showing dependence on aileron deflection for β=1.3° and α=34°.

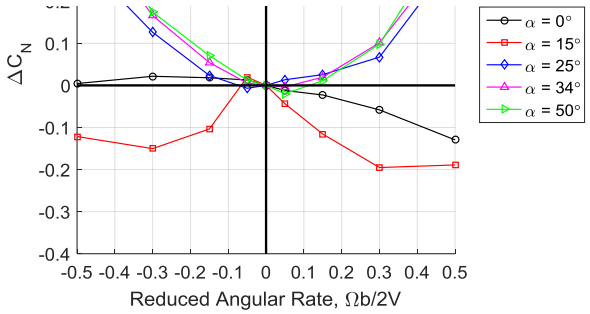

Figure 30. Effect of angle of attack on normal force coefficient, showing dependence on angle of attack and angular rate for β=1.3°.

The FASER rotary balance data were also analyzed using the steady state spin prediction method discussed earlier using the same control surface deflections as the spin observed during flight testing. **Error! Reference source not found.** shows the pitching moment equilibrium for the zero degrees sideslip orientation, with the inertial component calculated using Eq. 1. The aerodynamic components are represented by the blue lines and the inertial components are shown in red, with each line indicating a different angle of attack. **Error! Reference source not found.** lists these equilibrium points as well as the values for rolling moment that match these sideslip angles, angles of attack, and reduced angular rates. An example of the inertial and aerodynamic rolling moment equilibrium is shown in **Error! Reference source not found.**, with the inertial component calculated using Eq. 2. **Error! Reference source not found.** gives the angle of attack, reduced angular rate, and sideslip angles for these equilibrium points, as well as the corresponding inertial and yawing moment values. The inertial components are calculated from Eq. 2. The reduced angular rates and sideslip angles for each angle of attack are shown in **Error! Reference source not found.** and **Error! Reference source not found.**. These plots are used in order to quickly identify potential spin states. As shown in **Error! Reference source not found.**, the aerodynamic and inertial yawing moments intersect at one point. The aerodynamic yawing moment has a positive slope while the inertial yawing moment has a negative slope. Therefore, no equilibrium spin mode is predicted, which contradicts the spin mode observed and measured in flight data. Although it appears that there may be a stable equilibrium near 37 degrees angle of attack, though the aerodynamic data is too nonlinear for extrapolation and more analysis will be performed with the existing wind tunnel data to determine if additional wind tunnel data would allow the prediction of the spin mode seen in flight.

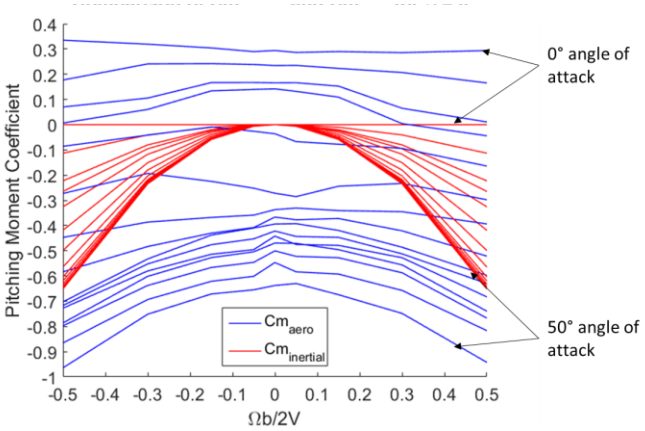

Figure 36. Aerodynamic (blue) and inertial (red) pitching moment equilibrium for a range of angles of attack for β=0°.

Table 4. Pitching moment equilibrium points and rolling moment values.

φ	α'	Equilibrium $\frac{\Omega b}{2V}$	Inertial C_l	Aero C_l
-5	15	-0.2574	-0.0013	0.0505
-5	20	-0.4039	-0.0043	0.0574
-5	25	0.4177	-0.0056	-0.0338
-5	30	0.4574	-0.0078	-0.0348
-5	34	0.4805	-0.0094	-0.0293
-5	36	0.4860	-0.0101	-0.0235
0	15	-0.1033	0	0.0221
0	20	-0.3449	0	0.0376
0	25	-0.4598	0	0.0516
0	30	0.4670	0	-0.0423
0	34	0.4951	0	-0.0404
10	15	0.0305	0.00006	-0.0228
10	20	-0.1947	0.0021	-0.0106
10	25	-0.3351	0.0071	0.0119
10	30	-0.4164	0.0130	0.0250
10	34	-0.4669	0.0177	0.0333
10	36	-0.4985	0.0208	0.0349

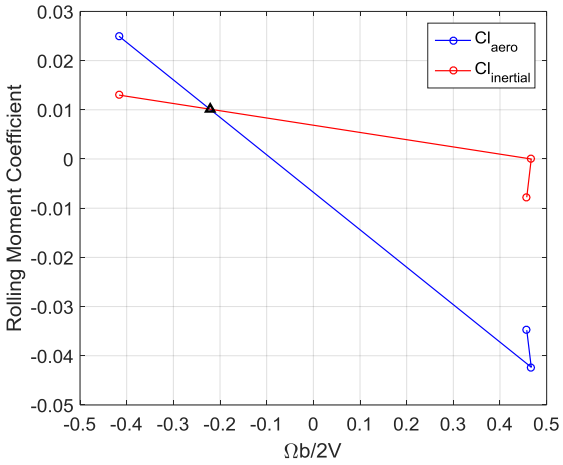

Figure 37. Aerodynamic and inertial rolling moment equilibrium for α=30°.

Table 5. Rolling moment equilibrium points and yawing moment coefficient values.

α'	$\frac{\Omega b}{2V}$	φ	Inertial C_n	Aero C_n
15	-0.0376	4.9075	0.00004	-0.0038
20	-0.2326	7.4820	0.0019	-0.0067
25	0.1076	-3.2332	-0.0002	-0.0160
30	-0.2218	7.7969	0.0017	0.0076
34	-0.1990	7.2156	0.0012	0.0104
36	0.0077	2.2877	0.000003	0.0017

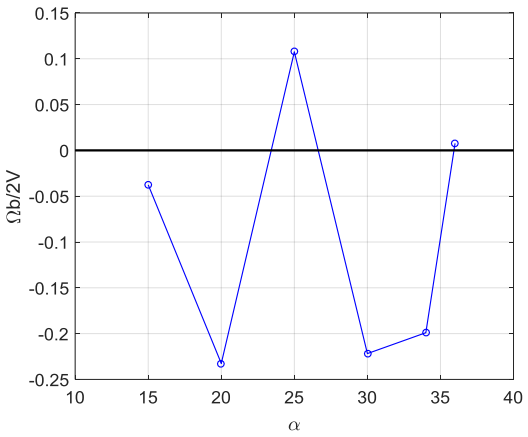

Figure 38. $\frac{\Omega b}{2V}$ vs α, from satisfying rolling moment equilibrium.

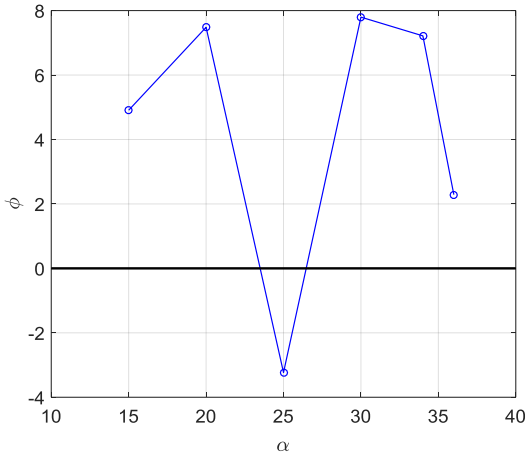

Figure 40. φ vs α, from satisfying rolling moment equilibrium.

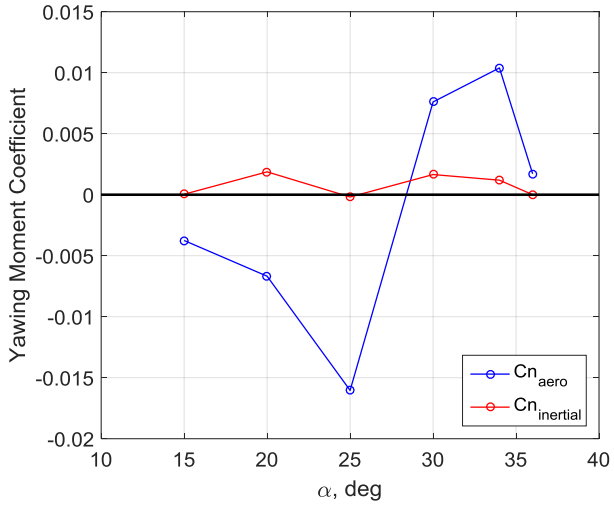

Figure 39. Aerodynamic and inertial yawing moment equilibrium for FASER, which does not show a steady-state spin mode, due to the greater slope of the aerodynamic component compared to the inertial.

V. Summary, Conclusions, and Future Work

A rotary balance test of the FASER research aircraft was conducted in the NASA LaRC 20-Foot Vertical Spin Tunnel. The FASER aircraft is used as an inexpensive and low risk UAV platform for flight dynamics research. A rotary balance wind tunnel test of the FASER aircraft was conducted in order to analyze the effects of rotary motion on aircraft dynamics, including the effects of angle of attack, sideslip angle, angular rate, and control surface deflection. Tests were performed at angles of attack from 0 to 50 degrees, sideslip angles of -5 to 10 degrees, and reduced angular rates from -0.5 to 0.5. The effects of pro-spin elevator and rudder deflection and pro- and anti-spin elevator, rudder, and aileron deflection were examined. The rotary balance data were also used in a steady state spin prediction tool to see if the rotary data could be used to predict the spin observed in flight tests. In addition to rotary data, static data were also measured in order to ensure that there were no anomalies in the vertical wind tunnel that required correction before the rotary balance test. The results from the rotary balance measurements demonstrated that:

1. Reynolds number effects are minimal between flight testing and tunnel conditions.
2. Aircraft force and moment coefficients have a functional dependence not only on angle of attack and sideslip angle, but also on angular rate.
3. The functional dependence of the rotary force and moment coefficients on control surface deflections is small and asymmetric with respect to angular rate. More investigation is necessary in order to fully characterize the effects of control deflections.
4. The steady state spin prediction method did not find the equilibrium spin mode that was observed in flight testing.

Future work will include updating the existing simulation aero database to include the experimental rotary balance data. This data will be a function of angle of attack, sideslip angle, angular rate, and, if necessary, control deflections. It will be used along with previous forced oscillation data to model post-stall aircraft characteristics. Future flight tests will provide additional data in order to verify the results of the steady state spin prediction and the simulation results.

Acknowledgments

The authors would like to thank the staff members in the NASA LaRC Flight Dynamics Branch who assisted greatly in conducting the wind tunnel test. This work was conducted as a part of the NASA LARSS and NIFS internship programs.

References

[1]Owens, D.B., Cox, D.E., and Morelli, E.A.; "Development of a Low-Cost Sub-Scale Aircraft for Flight Research: The FASER Project," AIAA 2006-3306, 25th AIAA Aerodynamic Measurement Technology and Ground Testing Conference, June 2006.

[2]Hoe, G., Owens, D.B., and Denham, C.; "Forced Oscillation Wind Tunnel Testing for FASER Flight Research Aircraft," AIAA 2012-4645, AIAA Atmospheric Flight Mechanics Conference, August 2012.

[3]Chambers, J.R.; "Modeling Flight: The Roll of Dynamically Scaled Free-Flight Models in Support of NASA's Aerospace Programs," NASA SP 2009-575, 2009.

[4]Bihrle, W., "Rotary Balance Techniques: Historical Background," AGARD-AR-265, 1990.

[5]Guglieri, G., and Quagliotti, F.B.; "Experimental Analysis of Rotary Derivatives on a Modern Aircraft Configuration," AIAA 1993-3514, 1993.

[6]Aaron, K.; "Rotary Balance Prediction of Aircraft Spin Modes," Master of Science Thesis, California Institute of Technology, September 1980.

[7]Owens, D.B., Brandon, J.M., Croom, M.A., Fremaux, C.M., Heim, E.H., and Vicroy, D.D.; "Overview of Dynamic Test Techniques for Flight Dynamics Research at NASA LaRC," AIAA 2006-3146, 25th AIAA Aerodynamic Measurement Technology and Ground Testing Conference, June 2006.

[8]Murch, A.M.; "Aerodynamic Modeling of Post-Stall and Spin Dynamics of Large Transport Airplanes," Georgia Institute of Technology, August 2007.

[9]Birhle, W. and Barnhart, B.; "Spin Prediction Techniques," AIAA 80-1564, 1980.